Real-Time Hand Motion-Modulated Chipless RFID With Gesture Recognition Capability

Ashkan Azarfar, Nicolas Barbot, Etienne Perret

Real-Time Hand Motion-Modulated Chipless RFID with Gesture Recognition Capability

Ashkan Azarfar, Nicolas Barbot, and Etienne Perret

***Abstract*—This paper presents a real-time identification process for slow motion-modulated chipless RFID which can be applied to human hand gestures to realize a full-practical long-range RFID system with gesture recognition capability. Depolarizing chipless tags configured by hand in three gestures are utilized while different motion-induced modulation effects involved in each gesture are analytically modeled. The identification based on differential RCS and gesture recognition using deterministic IQ trajectories is addressed according to the developed model. The fast reading process for slow motion-modulated chipless RFID is proposed based on the sequential fast frequency sweep acquisitions by VNA while the sweep time is very short compared to the period of motion. The identification time achieved using this approach is about only a few periods of motion which is ideal to implement hand gesture-modulated chipless RFID in real-time. The designed gesture-modulated chipless tag is identified during a few seconds at distances up to 3 m for the most efficient gesture. Moreover, all the hand gestures are recognized at 2 m range based on the received IQ signature. These achievements realize the practical example of motion-modulated chipless RFID where both tag identification and gesture recognition are simultaneously provided.**

***Index Terms*—Backscatter modulation, Differential Radar Cross Section (RCS), Hand gesture recognition, Motion-modulated chipless Radio Frequency IDentification (RFID)**

I. Introduction

CHIPLESS technology has been introduced to present a new low-cost paradigm for the RFID market based on the principle of excluding electronic chips from tags structure [1]–[3] which relatively alleviates the environmental impact of massive usage of RFID tags [4]. Chipless RFID has been well developed in aspects such as coding approach [5]–[7], coding capacity [8], [9], and detection robustness [10]–[13] while this technique essentially suffers from limited read ranges of less than 1 meter. In fact, since chipless tags have no source of modulation and behave as Linear Time-Invariant (LTI) systems, their backscattering response cannot be easily detected within the reflection from stationary background objects [14].

Based on the landmark idea of backscatter communication using moving reflectors presented by [15], [16], motion-modulated chipless RFID has been recently introduced in [17] where the time-variant feature of motion has been integrated with chipless technology to break the LTI property of chipless tags, and consequently, to significantly increase the reading distance. Indeed, moving chipless tags behave as Linear Time-Variant (LTV) transponders that modify the backscattered wave such that the modulated reflection from the tag is simply differentiated from the static reflection of the background environment which leads to read range enhancement [17]. Different kinds of motion-induced modulation such as load modulation [18], phase (or micro-Doppler [19]) modulation [20], [21], polarization modulation [22], and directional amplitude modulation [23] have been applied for motion-modulated chipless RFID up to now, where a reading distance of several meters has been achieved in all these works. Moreover, different motion sources such as mechanical rotation [18], [20], [21], [23], mechanical vibration [24], translation of conveyor belts [25], and natural vibration of human respiration [26] have been employed in motion-modulated chipless RFID.

The classical reading process for motion-modulated chipless RFID presented in [17] has been realized using a coherent transceiver implemented by a signal generator and a spectrum analyzer which are synchronized. According to the reading method in [17], the coherent transceiver should change its operating frequency sequentially to measure the differential backscattered power (the modulated power around each carrier frequency which defines the differential RCS [27], [28]) at all required frequency points over the coding bandwidth of the chipless tag. Accordingly, the obtained differential RCS as a function of carrier frequency shows peaks associated with resonance frequencies of the chipless tag which provides the identification capability. However, based on the classical reading method, for relatively large coding bandwidths and so large number of sequential measurements, the total time duration needed to identify the tag, called identification time, can be very long, especially for slow movements like human motions. Thus, although the total identification time has not been addressed in [25], [26], a quite long identification time of a few minutes can be expected in these works. This fact demonstrates that the classical reading approach cannot be feasibly applied for motion-modulated chipless RFID based on natural slow motions (e.g. human body movements) which can be the most common cases for real scenarios. Recently, a more time-efficient reading process compared to the classical approach in motion-modulated chipless RFID has been proposed in [29]. The technique is based on a complex reader bench composed of a wideband vector signal generator and a wideband real-time spectrum analyzer, while the identification time is still more than one minute. In addition, a fast reading process for motion-modulated chipless RFID has been introduced in [30] based on the Vector Network Analyzer (VNA) measurement in frequency-offset mode whereas it can be applied only for rapid motions and not for natural slow movements.

Human hand motions, called hand gestures, are one of the most common natural movements that have been applied for wireless human-machine communication. Hand gesture

The authors are with the University of Grenoble Alpes, Grenoble INP, LCIS, F-26000 Valence, France (email: ashkan.azarfar@lcis.grenoble-inp.fr).
This is an extended version of the original conference paper at IMS 2024.

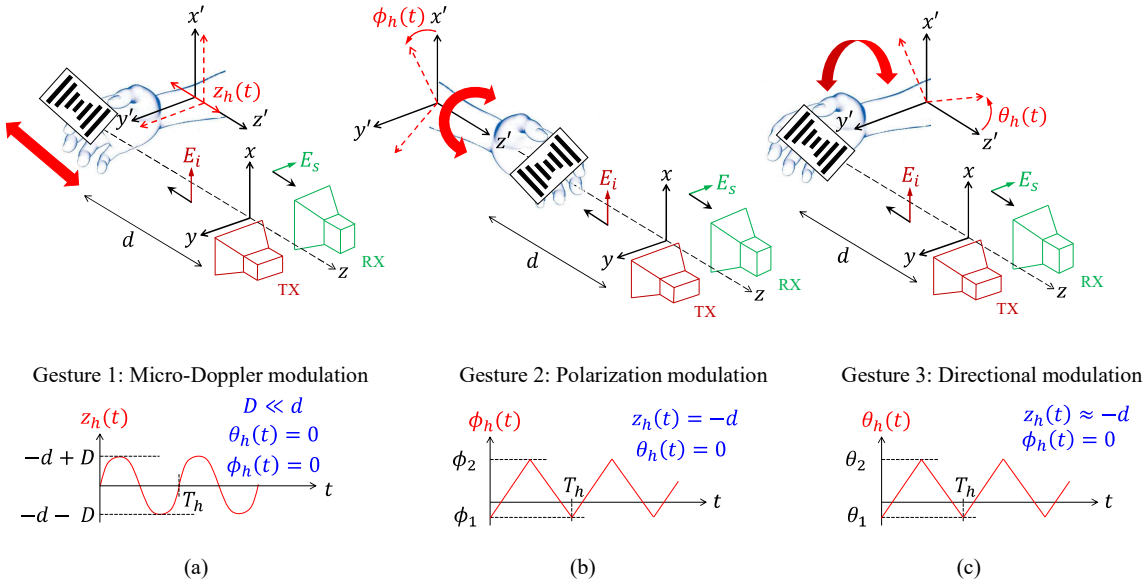

Fig. 1. Three considered human hand gestures to realize motion-modulated chipless RFID based on different modulation effects. (a) Gesture 1 is to linearly shake the hand where the main modulation effect is micro-Doppler. (b) Gesture 2 is to turn the hand in azimuth direction where the main modulation effect is polarization modulation. (c) Gesture 3 is to turn the hand in elevation direction where the main modulation effect is directional amplitude modulation.

recognition based on micro-Doppler radar approaches has been investigated in [31]–[37] (with the prominent example of Google Soli [31]) where feature vectors are extracted in the time-frequency domain using micro-Doppler measurement in each hand gesture, and then classified based on Convolutions Neural Networks (CNN) approach. Worth mentioning that, the feature extraction process in all these works [31]–[37] is not based on analytical approaches to predict the backscattering signature of the hand in different gestures, but derived by complex machine learning techniques to extract the gesture information. Moreover, the achieved read range in [31]–[37] is not more than several 10 cm. The classical chipless RFID technology has been also applied for gesture recognition in [38]–[40] and [41] respectively based on touch-sensing and phase multi-lateration approaches whereas the time-variant property of the hand motion has not been involved in the recognition process, which causes to have the same limited read range of 30 cm as classical chipless RFID. However, hand gestures have a good potential to be applied for motion-modulated chipless RFID [42], provided that a fast reading process is realized such that slowly moving chipless tags can be identified in a few seconds. In addition to providing identification capability at large distances, the motion-modulated backscattering signature of the moving chipless tags can be analytically obtained, in contrast to that of the hand itself, which yields the gesture recognition possibility without a database collection process.

This paper, as an extended version of [42], presents a full-practical motion-modulated chipless RFID system based on a fast frequency sweep reading process which is applied for held-in-hand chipless tags modulated by different hand gestures. In the proposed fast reading approach, the motion-modulated signal samples associated with all the required frequency points are captured by a sequence of fast frequency sweep acquisitions during several periods of motion which provides all the data needed for differential RCS calculation and identification of tags at large distances. Moreover, the analytically obtained backscattering In-phase/Quadrature (IQ) signature of the hand gesture-modulated chipless tags is utilized for gesture recognition which adds another way to communicate with the reader in addition to the tag identification.

The paper is organized as follows. Section II presents the analytical model for motion-modulated wave backscattered from the designed chipless tag in three different hand gestures, while the tag identification and the gesture recognition capability are demonstrated based on the model. Section III describes the proposed fast reading process for slow motion-modulated chipless tags in comparison with the classical reading approach, where both methods are implemented using VNA measurements and the great identification time reduction provided by the proposed fast approach is demonstrated. Section IV presents the measurement bench and discusses the results in terms of identification time, read range, and gesture recognition capability. Finally, Section V concludes the paper.

II. Analytical Model

The three different hand gestures utilized for motion-modulated chipless RFID are illustrated in Fig. 1 where a RF Encoding Particle (REP)-based chipless tag [43] with a size comparable to a credit card is held in hand during each gesture. The human hand is assumed to perform the gestures at a distance of d from cross-polarized transmitting (TX) and receiving (RX) antennas. The incident field from the TX antenna is vertically (x) polarized and the RX antenna is horizontally (y) polarized. The reference coordinate system (CS) xyz is attached to the antennas and the local CS $x'y'z'$ is attached to the hand to describe the approximated hand motion in each gesture and the tag configuration.

A. Chipless Tag Design

The considered REP-based chipless tag in this work is inspired by the structure presented in [44]. While in [44] each resonant REP consists of multiple strip dipoles, the proposed chipless tag here is composed of single grounded-dipole REPs as shown in Fig. 2 (a) and (b). The strip dipole has a length of l, width of w, and a thickness of h_d which is printed on a grounded dielectric substrate with permittivity of ϵ_r, the length of l_s, width of w_s, and thickness of h_s. The chipless tag consisting of grounded-dipole REPs can be arranged in a 45° tilted configuration respect to the x-polarized incident field as it is shown in Fig. 2 (c) to realize a depolarizing configuration. In fact, supposing that the hand itself does not have any strong cross-polarized backscattering component, using the depolarizing chipless tags leads to suppress the backscattering from the hand in reception, and so, increase the detection robustness of motion-modulated chipless tags [25], [26]. In addition, due to the grounded structure of the tag, the electromagnetic coupling between the tag and hand is significantly suppressed. Consequently, as far the grounded-dipole resonators are not directly touched by hand (e.g. by fingers) and the tag is held from the substrate edge (as shown in Fig. 1), the presence of the hand does not perturb the tag performance which leads to improving the detection robustness. As it is shown in Fig. 1, the x-polarized incident plane wave at the frequency of f_0 can be expressed as

$$\vec{E}_i(z) = E_x^i \, \hat{x} \, e^{jkz} \tag{1}$$

where $k = 2\pi f_0/c_0$ and c_0 is the free-space light velocity. Assuming the chipless tag is positioned by hand in its initial depolarizing stationary state as shown in Fig. 1 and Fig. 2 (c), the spherical backscattered wave is written as

$$\vec{E}_s(z) = (E_x^s \, \hat{x} + E_y^s \, \hat{y}) \, \frac{e^{-jk(z+2d)}}{z+d} \tag{2}$$

where d is the distance between the tag and the reception point, and the co/cross (E_x^s and E_y^s) field components are obtained based on the polarimetric scattering matrix in terms of the incident field components expressed as

$$\begin{bmatrix} E_x^s \\ E_y^s \end{bmatrix} = \begin{bmatrix} S_{xx}(f_0) & S_{xy}(f_0) \\ S_{yx}(f_0) & S_{yy}(f_0) \end{bmatrix} \begin{bmatrix} E_x^i \\ E_y^i \end{bmatrix} \tag{3}$$

Worth mentioning that, the backscattered field obtained by (2) and (3) is associated with the initial depolarizing configuration of the held-in-hand chipless tag, which is assumed to be preserved during all hand gestures.

For $l_s = 50$ mm, w_s=30 mm, $h_s = 0.5$ mm, $h_d = 0.01$ mm, $w = 2.5$ mm, and $\epsilon_r = 2.2$ the structure of the proposed chipless tag is analyzed using Ansys HFSS full-wave simulation. For $l = 24$ mm, the current distribution on the depolarizing grounded-dipole at the first resonant mode ($f_0 = 4.14$ GHz) is shown in (Fig. 2) (d). The simulated cross-polarized scattering parameter $S_{yx}(f)$ of the single-REP tag for different dipole lengths ($l = 18, 20, 22, 24$ mm) is illustrated in (Fig. 2) (e) as a function of frequency where clearly separated resonant peaks associated to each length demonstrate how to design a multi-REP chipless tag (e.g. the one shown in hand in Fig. 1).

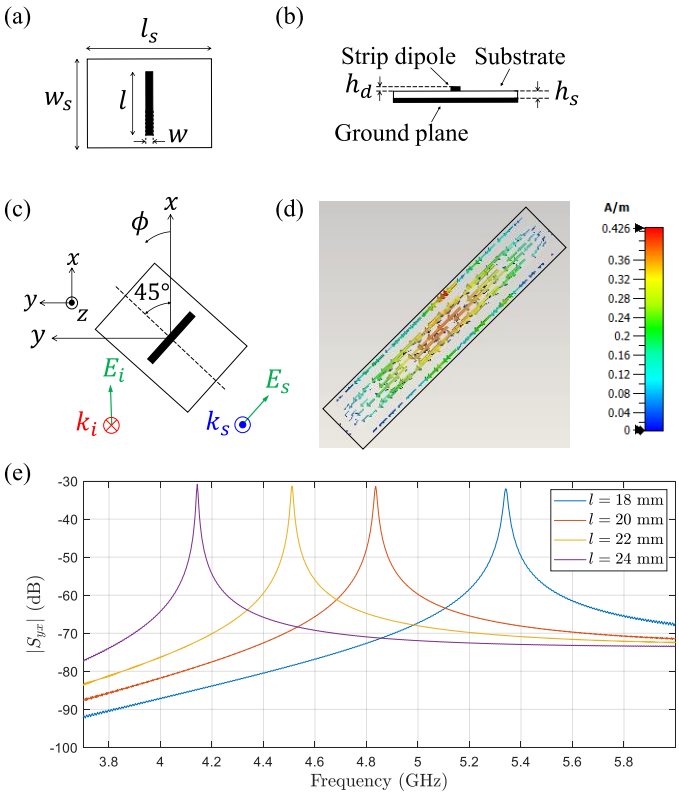

Fig. 2. (a) Top view (b) Side view of single-REP chipless tag with grounded-dipole resonator. (c) Backscattering from depolarizing configuration of the chipless tag. (d) Surface current distribution on the depolarizing grounded-dipole at the dominant resonant mode. (e) Cross-polarized scattering parameter of 45° tilted grounded-dipole for different lengths as a function of frequency

According to the desired coding capacity, the number of grounded-dipole REPs on the tag and their respective lengths can be easily obtained using similar full-wave simulations.

B. Hand Gestures Description

Generally, hand gestures can be a combination of rotational and vibrational motion respect to different axes. The three hand gestures here are considered such that in each gesture the motion can be approximated with either a single periodic vibration or single periodic rotation with a period of T_h. Note that, the period of all gestures should not be necessarily equal, however, for the sake of simplicity the motion period T_h is assumed to be same for all gestures. Accordingly, the approximated hand motion trajectory in each gesture are described as follows.

1) Gesture 1:

As it is shown in Fig. 1 (a), in Gesture 1, the human hand is linearly shaken along z axis with an amplitude of $D \ll d$ while the initial depolarizing configuration of the chipless tag does not change during the hand movement. Thus, the motion trajectory of the chipless tag can be approximated as

$$z_h(t) \approx -d + D \sin(2\pi f_h t) \tag{4}$$

where $f_h = 1/T_h$. Since it is assumed that the human hand does not undergo any rotation during this gesture, the azimuth $\phi_h(t)$ and elevation $\theta_h(t)$ angle of the chipless tag during time

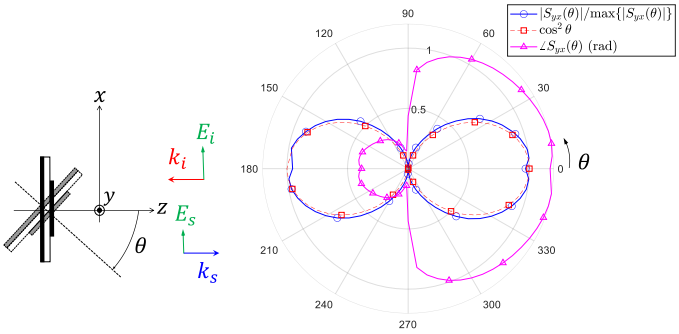

(a) (b)

Fig. 3. (a) Side view of backscattering from the chipless tag while rotates in elevation direction. (b) Normalized magnitude and phase of the cross-polarized scattering parameter of the chipless tag while rotates in elevation direction.

is approximated to be constant as $\phi_h(t) = 0$ and $\theta_h(t) = 0$. The corresponding sketch of $z_h(t)$ in Gesture 1 is shown in Fig. 1 (a).

2) Gesture 2:

As it is shown in Fig. 1 (b), in Gesture 2, the human hand is turned around z axis (around the elbow joint) such that its azimuth angle variation can be approximated as

$$\phi_h(t) \approx \phi_1 + \phi_2 \sum_{n=0}^{+\infty} \Lambda[\frac{t-(n+\frac{1}{2})T_h}{\frac{1}{2}T_h}] \tag{5}$$

where $\Lambda(t)$ is the common triangular function, and ϕ_1 and ϕ_2 are the extreme rotation angles around the elbow joint that can be reached respectively in clockwise and counter-clockwise directions. Since it is assumed that the human hand is fixed in distance and does not undergo any rotation around the y axis, the relative distance $z_h(t)$ and the elevation angle $\theta_h(t)$ are assumed to be constant as $z_h(t) = -d$ and $\theta_h(t) = 0$ in this gesture. The corresponding sketch of $\phi_h(t)$ in Gesture 2 is shown in Fig. 1 (b). Note that, the angular variation $\phi_h(t)$ is considered to be linear as a first order approximation which will be useful to accomplish the analytical expression of the motion-modulated backscattered field.

3) Gesture 3:

As it is shown in Fig. 1 (c), in Gesture 3, the human hand is turned around y axis such that its elevation angle variation can be approximated as

$$\theta_h(t) \approx \theta_1 + \theta_2 \sum_{n=0}^{+\infty} \Lambda[\frac{t-(n+\frac{1}{2})T_h}{\frac{1}{2}T_h}] \tag{6}$$

where θ_1 and θ_2 are the extreme rotation angles around the elbow joint that can be reached respectively in forward and backward directions. Since it is assumed that the human hand is fixed in distance and does not undergo any rotation around the z axis, the relative distance $z_h(t)$ and the azimuth angle $\phi_h(t)$ are assumed to be constant as $z_h(t) = -d$ and $\phi_h(t) = 0$ in this gesture. The corresponding sketch of $\theta_h(t)$ in Gesture 3 is shown in Fig. 1 (c) while the same linear approximation is assumed for $\theta_h(t)$.

C. Motion-Modulated Backscattered Field

The motion-induced modulation on the backscattered wave from a moving chipless tag depends on the motion trajectory and how resonant REPs on the chipless tag change their configuration respect to the incident field during motion [17]. The different kinds of modulation effects caused by a moving chipless tag have been addressed as micro-Doppler modulation for rotating [21] and vibrating tags [23], polarization modulation for rotating tags [22], and directional amplitude modulation for rotating tags [24]. In contrast to [17], [22]–[24] where the utilized motion source is implemented based on mechanical setups with motors and loudspeakers, all kinds of presented motion-induced modulation effects in [22], [23] and [24] are respectively realized in Gesture 1, Gesture 2, and Gesture 3 using the natural hand motion which can be easily applied in real RFID scenarios. In addition, motion-modulated chipless tags in [23], [24] are configured in non-depolarizing configuration that limits the detection performance depending on the tagged object geometry. However, the depolarizing configuration easily realized by hand in Gesture 1 and Gesture 3 which significantly increases the detection robustness here. According to the theoretical model developed in [22]–[24], the corresponding cross-polarized component (y component) of the motion-modulated backscattered field in each gesture are obtained as follows.

1) Gesture 1: Due to the linear vibrational motion of the hand in Gesture 1 given by (4), the main involved motion-induced modulation effect in this gesture is the vibrational micro-Doppler which only modulates the phase of the backscattered wave in $+z$ direction expressed as [21]

$$E_y^{s^{(1)}}(z,t) = S_{yx}(f_0)\, E_x^i\, \frac{e^{-jk(z+2d)}}{z+d}\, e^{j\beta \sin(2\pi f_h t)} \tag{7}$$

where $\beta = 4\pi D/\lambda$ is the micro-Doppler modulation index and $S_{yx}(f_0)$ is the cross-polarized scattering parameter of the chipless tag given in (3). Note that, in contrary to [23], [26] where the vibrational displacement (less than a few millimeters) is very small compared to the operating wavelength resulting in very small modulation index ($D_{vib}/\lambda \ll 1 \rightarrow \beta \ll 1$), the hand displacement (more than several centimeters) in Gesture 1 can provide very large modulation index which enhance both differential RCS and read range, as it will be shown in next parts.

2) Gesture 2: The azimuthal rotation of a chipless tag in a plane normal to the incident wave direction has been demonstrated in [22] to modulate the backscattered wave only in terms of polarization. Accordingly, the motion-modulated backscattered field in Gesture 2 based on the approximated rotational trajectory in (5) can be obtained as [22]

$$E_y^{s^{(2)}}(z,t) = S_{yx}(f_0)\, E_x^i\, \frac{e^{-jk(z+2d)}}{z+d}\, \cos[2\phi_h(t)] \tag{8}$$

where the magnitude of the backscattered wave is modulated proportional to the azimuthal rotation. Worth mentioning that, the rotation considered in [22] is continuous with a single direction while the hand rotation in Gesture 2 is in both

clockwise and counter-clockwise directions between the two extreme angles of ϕ_1 and ϕ_2.

3) Gesture 3: The concept of directional amplitude modulation in backscattering from moving scatterers has been addressed in [24] based on Doppler suppression due to the resonance effect. In fact, this modulation effect is caused by the reradiation pattern of a scatterer during rotation. Accordingly, the rotation of the chipless tag in elevation during Gesture 3 can modulate the magnitude of the backscattered wave proportional to the reradiation pattern of the grounded-dipole REP. However, in Gesture 3 the phase modulation caused by the rotation is not completely suppressed like what has been discussed in [24]. In addition, the reradiation pattern of the grounded-dipole REP cannot be analytically derived as in [24]. Accordingly, to obtain an approximation for the motion-modulated backscattered field in Gesture 3, the variation of the magnitude and the phase of the cross-polarized backscattered field while the tag is rotated around y-axis as shown in Fig. 3 (a), is calculated using Ansys HFSS full-wave simulation. The simulation results are shown in Fig. 3 (b) as a function of rotation angle θ at the resonance frequency of the grounded-dipole REP $l = \lambda/2$. As it is illustrated in Fig. 3 (b), the normalized magnitude of $S_{yx}(\theta)$ can be well approximated as $\cos^2\theta$ while the phase variation $\angle S_{yx}(\theta)$ is observed due to the small rotational displacement. Nevertheless, since the phase variation is less significant compared to the magnitude variation, the motion-modulated backscattered field in Gesture 3 can be approximated by considering only the directional amplitude modulation, which is expressed as [24]

$$E_y^{s^{(3)}}(z,t) \approx S_{yx}(f_0)\, E_x^i\, \frac{e^{-jk(z+2d)}}{z+d}\, \cos^2\theta_h(t) \tag{9}$$

Note that, similar to Gesture 2, the rotation in Gesture 3 is a bidirectional rotation, in contrast to [24], which is limited between the two extreme angles of θ_1 and θ_2.

D. Chipless Tag Identification Based on Differential RCS

The original concept of differential RCS has been introduced for UHF RFID tags in [27] which shows how much the used electronic chip can effectively modulate the backscattered wave based on the load modulation. After that, the definition of the differential RCS has been generalized in [28] for any kind of LTV transponders. Based on the general definition given by [28], the differential RCS of the motion-modulated chipless tags has been derived in [17] based on the both time-domain and frequency-domain analysis of the backscattered field or the received signal. Accordingly, the differential RCS of the hand gesture-modulated chipless tags can be calculated in each gesture using (7)-(9).

By looking at the obtained expressions for motion-modulated backscattered field in Gesture 1, Gesture 2, and Gesture 3 respectively shown by (7), (8), and (9), a general expression can be proposed for motion-modulated backscattered field that is fitted to all the gestures presented here and is written as

$$E_y^{s^{(p)}}(z,t) = S_{yx}(f_0)\, E_x^i\, \frac{e^{-jk(z+2d)}}{z+d}\, \psi^{(p)}(t) \tag{10}$$

where $\psi^{(p)}(t)$ for $p = 1,2,3$ is the complex periodic modulation function respectively in Gesture 1 , Gesture 2, and Gesture 3. According to the time-domain definition of the differential RCS in [28], the general expression of the differential RCS for all three hand gesture-modulated chipless tags is obtained using (1) and (10) that is expressed as

$$\sigma_d^{(p)}(f_0) = \frac{4\pi d^2}{T_h}\, \frac{\int_0^{T_h} |E_y^{s^{(p)}}|^2\, dt - |\int_0^{T_h} E_y^{s^{(p)}}\, dt|^2}{|E_x^i|^2} \tag{11}$$

where $E_y^{s^{(p)}} = E_y^{s^{(p)}}(z=0,t)$. Then, equation (11) can be rewritten as

$$\sigma_d^{(p)}(f_0) = 4\pi |S_{yx}(f_0)|^2\, (e_n[\psi^{(p)}] - |a_0[\psi^{(p)}]|^2) \tag{12}$$

where

$$e_n[\psi^{(p)}] = \frac{1}{T_h} \int_0^{T_h} |\psi^{(p)}(t)|^2\, dt \tag{13}$$

$$a_0[\psi^{(p)}] = \frac{1}{T_h} \int_0^{T_h} \psi^{(p)}(t)\, dt \tag{14}$$

are respectively the norm and the average of the complex modulation function $\psi^{(p)}(t)$ in each gesture for $p = 1,2,3$. Based on the approximated motion trajectories in each gesture given by (4)-(6), the analytical expression of $e_n(\psi)$ and $a_0(\psi)$ for each gesture is calculated in terms of gesture characteristics using (13) and (14) which are indicated in Table I. Note that, the general expression of the differential RCS for hand gesture-modulated chipless tags given in (12) can be also calculated using the frequency-domain representation of the motion-modulated backscattered field based on

$$\sigma_d^{(p)}(f_0) = 4\pi d^2\, \frac{\int_{-\infty}^{-\epsilon} |\mathbf{E}_y^{s^{(p)}}|^2\, df + \int_{+\epsilon}^{+\infty} |\mathbf{E}_y^{s^{(p)}}|^2\, df}{|E_x^i|^2} \tag{15}$$

where $\mathbf{E}_y^{s^{(p)}} = \mathbf{E}_y^{s^{(p)}}(z=0,f)$ is the time Fourier transform of $E_y^{s^{(p)}}(z=0,t)$ for $p = 1,2,3$ and $[-\epsilon,\epsilon]$ is the zero-excluding integration bandwidth to remove the static portion of the backscattered power located at $f = 0$. It can be shown that (15) yields the same general expression as (12) for the differential RCS of the hand gesture-modulated chipless tags.

Worth mentioning that, equation (12) clearly demonstrated how the identification data encoded into the backscattering frequency response of the stationary chipless tag $|S_{yx}(f_0)|^2$ is translated into the differential RCS response of the hand gesture-modulated chipless tag using the motion induced modulation. Thus, the identification capability is clarified by (12). In addition, the key factor which shows how much the motion-induced modulation is efficient can be defined as Motion-Induced Modulation Efficiency (MIME) expressed as

$$\text{MIME}[\psi^{(p)}] = e_n[\psi^{(p)}] - |a_0[\psi^{(p)}]|^2 \tag{16}$$

for $p = 1,2,3$ corresponding to Gesture 1, Gesture 2, and Gesture 3. For the typical gesture characteristics indicated in

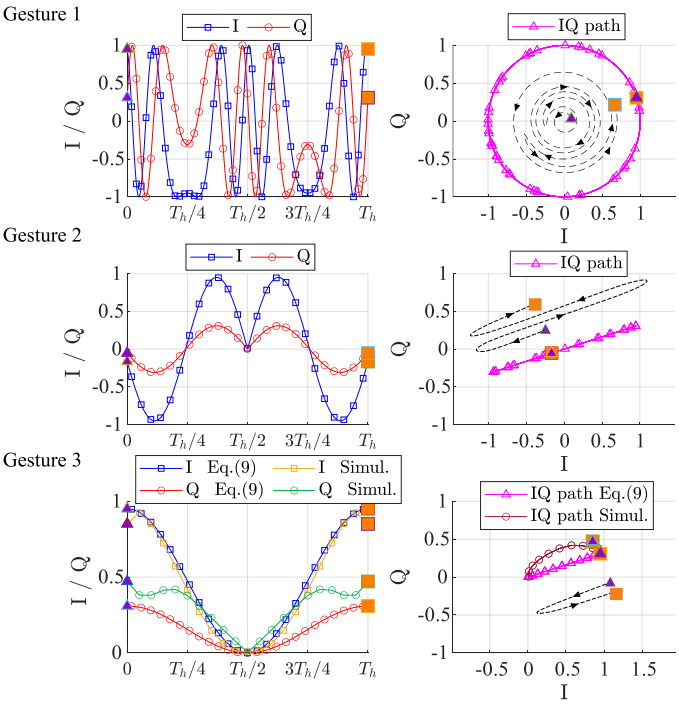

Fig. 4. Normalized IQ components of the motion-modulated backscattered field in three gestures obtained from model. The IQ variation during one period is shown at the left and the corresponding IQ paths and IQ trajectories are shown at the right.

Table II, the value of MIME is noted for the three gestures which demonstrates that Gesture 1 has the most efficient motion-induced modulation while Gesture 3 is not so efficient for motion-modulated chipless RFID. Accordingly, with an equal transmitted power level for all gestures, Gesture 1 is expected to provide the largest reading distance for the motion-modulated chipless tag, while Gesture 2 and Gesture 3 are respectively placed at the second and third rank. However, note that the MIME in Gesture 1 depends on the operating frequency band whereas the MIME in Gesture 2 and Gesture 3 are independent of frequency, which can be taken into account as an advantage for these two gestures.

E. Gesture Recognition Based on IQ Signature

Based on the obtained analytic expression of the motion-modulated field backscattered from the hand gesture-modulated chipless tag in (7), (8), and (9) respectively associated with Gesture 1, Gesture 2, and Gesture 3, the deterministic time domain IQ signature of the moving chipless tag can be derived in each gesture which is utilized for hand gesture recognition. Accordingly, the normalized IQ components of the motion-modulated backscattered field $I(t) = \text{real}\{E_y^{s(p)}/\max(|E_y^{s(p)}|)\}$ and $Q(t) = \text{imag}\{E_y^{s(p)}/\max(|E_y^{s(p)}|)\}$ for $p = 1, 2, 3$ are obtained based on (7)-(9) and they are shown in Fig. 4 during one period of gesture. In addition, Fig. 4 presents the corresponding IQ diagram for each gesture where the IQ paths are shown in pink color and the IQ trajectories are illustrated by the black dashed line in each case. In fact, the IQ path shows where the IQ points are located in the IQ diagram while

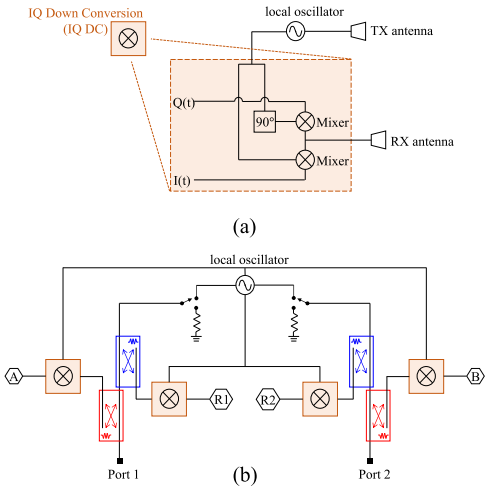

Fig. 5. (a) Basic architecture of a coherent IQ transceiver. (b) Schematic illustration of the internal architecture of a two-port VNA.

the IQ trajectory shows how the IQ path is followed by the signal during time. To make a relation between the values and positions of the IQ components along the IQ paths and the IQ trajectories in Fig. 4, the start and stop points are respectively marked with triangle and square marker while the direction of follow is indicated by arrows on the IQ trajectories. Note that, for Gesture 3 the data obtained from both the analytical expression in (9) and that from simulation are shown in Fig. 4 where the agreement between the results verifies the approximated directional amplitude modulation in Gesture 3. The IQ trajectories shown in Fig. 4 associated with the three gestures can be clearly recognized from each other which proves the gesture recognition capability based on hand gesture-modulated chipless RFID. Worth mentioning that, in contrast to the methods presented in [31]–[37], the feature vectors applied for CNN-based classifier (IQ trajectories here) can be analytically determined in motion-modulated chipless RFID. In other words, a simple classifying algorithm such as Support Vector Machine (SVM) can be directly applied to the analytically obtained IQ trajectories (without needing a huge data collection process for feature extraction) to realize gesture recognition based on held-in-hand chipless tags. Moreover, the proposed approach can be applied to any more complex gestures since all possible motion-induced modulations due to hand gestures can be considered as a combination of the three considered modulation effects respectively in Gesture 1 to 3 [17].

III. Reading Process

A. Classical Approach

The basic reader architecture that can be used to identify LTV transponders such as UHF RFID tags and motion-modulated chipless RFID tags is shown in Fig. 5 (a) where a coherent IQ transceiver with a single local oscillator is employed to retrieve the data signal from the modulated carrier. In motion-modulated chipless RFID, to measure the differential RCS of the tag at N frequency points, the reader should change its operating frequency sequentially (for N

TABLE I
MOTION-INDUCED MODULATION FUNCTION FOR HAND GESTURES

	$\psi(t)$	$e_n(\psi)$	$a_0(\psi)$
Gesture 1	$e^{j\beta\sin(2\pi f_h t)}$	1	$J_0(\beta)$
Gesture 2	$\cos[2\phi_h(t)]$	$0.5+\frac{\sin(4\phi_2)-\sin(4\phi_1)}{8(\phi_2-\phi_1)}$	$\frac{\sin(2\phi_2)-\sin(2\phi_1)}{2(\phi_2-\phi_1)}$
Gesture 3	$\cos^2\theta_h(t)$	$0.375+\frac{[\sin(4\theta_2)-\sin(4\theta_1)]+8[\sin(2\theta_2)-\sin(2\theta_1)]}{32(\theta_2-\theta_1)}$	$0.5+\frac{\sin(2\theta_2)-\sin(2\theta_1)}{2(\theta_2-\theta_1)}$

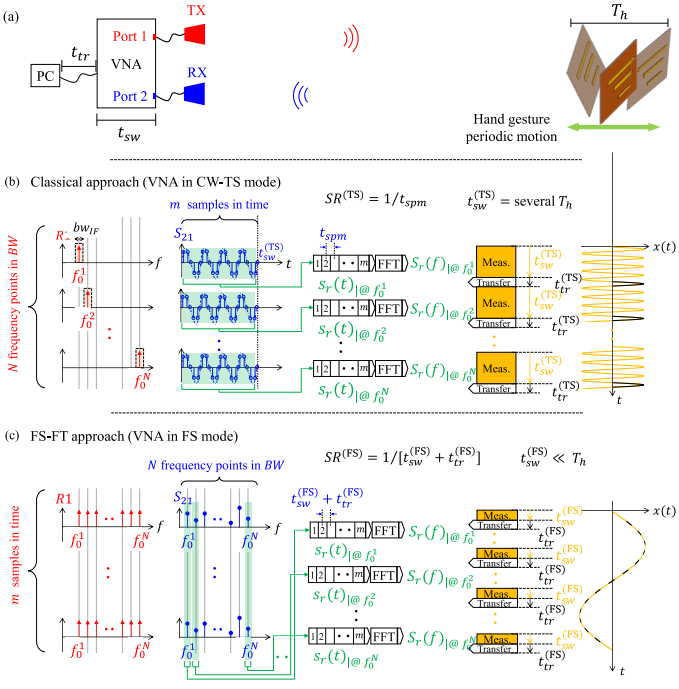

Fig. 6. (a) Proposed reader bench for motion-modulated chipless RFID using VNA. (b) Classical reading approach in motion-modulated chipless RFID realized by VNA. (c) Fast reading process for slow motion-modulated chipless RFID realized based on FS-FT approach using VNA.

times) to acquire the modulated backscattered power around each carrier frequency. This is the classical reading approach for motion-modulated chipless RFID which has been realized using a signal generator and a spectrum analyzer in [17], [21], [23]–[26], [29]. Since the signal generator and the spectrum analyzer work based on their own independent local oscillators, the two instruments have been synchronized in [17], [21], [23]–[26], [29] using a common reference signal to realize a coherent transceiver. Worth mentioning that, the total identification time t_{ID} (the time required to measure differential RCS of the motion-modulated chipless tag over its whole coding bandwidth BW at N frequency points) has not been addressed in none of these works [17], [21], [23]–[26], [29].

B. VNA Measurement Modes

The schematic internal architecture of a 2-port VNA is illustrated in Fig. 5 (b) where four coherent IQ transceivers have been configured with the directional couplers such that reference incident signals ($R1$ and $R2$) and reflected signals (A and B) are respectively measured in Port 1 and Port 2 of the VNA. Although the local oscillator of a VNA commonly works in frequency-sweep (FS) mode, it can be also fixed at one specific frequency while the port signals ($R1$, $R2$, A , B) are measured during time. This operation mode of a VNA is usually called CW-Time sweep mode (here called as CW-TS mode) or zero-span mode. Accordingly, a VNA in the CW-TS mode can be perfectly used to realize the classical reading process for motion-modulated chipless RFID presented in [17], [21], [23]–[26], [29], while there is no need for external synchronizing reference.

TABLE II
MODULATION EFFICIENCY OF HAND GESTURES

	Hand gesture characteristics	MIME
Gesture 1	$D = 5$ cm ($@f_0 = 4.5$ GHz)	0.97
Gesture 2	$\phi_1 = -135°$ $\phi_2 = 45°$	0.52
Gesture 3	$\theta_1 = 0°$ $\theta_2 = 90°$	0.125

The proposed reader bench based on VNA for motion-modulated chipless RFID is shown in Fig. 6 (a) where the TX and RX antennas are respectively connected to the Port 1 and Port 2 of the VNA, and the data transfer operation is controlled by a PC. The hand gesture-modulated chipless tag with the motion period of T_h is assumed at the distance of d from the antennas. To optimize the VNA measurement performance in terms of phase noise, the bistatic configuration with the measurement of $[S_{21}]$ scattering parameter is proposed here. In fact, the ratioed parameter $S_{21} = B/R1$ leads to a kind of phase noise cancellation due to the ratio process. Basically in a VNA, the time duration associated with the single point measurement t_{spm}, regardless of being in FS or CW-TS mode, is directly proportional to the Intermediate-Frequency (IF) bandwidth bw_{IF} which is set on the VNA. Accordingly, for VNA measurement in CW-TS mode, t_{spm} determines the acquisition sampling rate of the motion-modulated signal. In addition, the IF bandwidth bw_{IF} directly affects the signal-to-noise ratio (SNR) of the measurement which should be taken into account in the reading process. As it is shown in Fig. 6 (a), to address the identification time in the proposed reader bench based on VNA, there are two main time intervals that should be considered: the acquisition time corresponding to the sweep time t_{sw} taken by the VNA and the transfer time t_{tr} to send data from the VNA to the PC. The transfer time t_{tr} includes both times associated with the data transfer itself and also the data storage time on the PC, which depends on the used communication protocol between the VNA and the PC and can vary from a few milliseconds to several hundred milliseconds for different data sizes.

C. Classical Reading Approach Based on VNA

Fig. 6 (b) shows the classical reading approach for motion-modulated chipless RFID based on VNA measurement in CW-TS mode, which corresponds to the method presented in [17], [21], [23]–[26], [29] based on the synchronized signal generator-spectrum analyzer bench. Supposing that the differential RCS of the motion-modulated chipless tag is requested in N frequency points f_0^i, $i = 1, 2, ..., N$, the VNA in CW-TS mode sequentially (one by one) generates each carrier frequency at Port 1 while the $[S_{21}]$ scattering parameter is acquired at Port 2 during $t_{sw}^{(TS)}$ sweep time with a sampling rate of $SR^{(TS)} = 1/t_{spm}$. The power of carriers is defined by the output power P_t at Port 1. The sequentially transmitted carriers are shown as $R1(f)$ with red impulses in Fig. 6 (b) and the corresponding measured $[S_{21}]$ at each carrier frequency are shown as $S_{21}(t)$ with blue color in Fig. 6 (b). The IF bandwidth bw_{IF} set on the VNA should respect the Nyquist–Shannon sampling criterion based on the maximum frequency of the motion-modulated signal (up to several times of f_h). In addition, to provide sufficient number of samples in time and consequently sufficient frequency resolution, the sweep time $t_{sw}^{(TS)}$ should lasts for at least several periods of motion ($t_{sw}^{(TS)}$ = several T_h) [shown by yellow color on the motion trajectory in Fig. 6 (b)] while the data transfer time $t_{tr}^{(TS)}$ lasts for only a small portion of period [shown by black color on the motion trajectory in Fig. 6 (b)]. Obviously, during the transfer time $t_{tr}^{(TS)}$, the classical reading process miss the motion-modulated signal since it is not acquired by the VNA. At each carrier frequency (N carrier frequencies), the signal samples (m samples) are acquired during time by the VNA. The acquired data is transferred to the PC and then is arranged in rows as it is shown by shaded green bars and green paths in Fig. 6 (b) to form the complex motion-modulated received signal as

$$s_r(t_q)\Big|_{@\, f_0^i} = \sqrt{P_t}\, S_{21}(t_q)\Big|_{@\, f_0^i} \tag{17}$$

for $q = 1, 2, ..., m$ and $i = 1, 2, ..., N$ where $t_q = (q-1)\, t_{spm}$. The Power Spectral Density (PSD) of the motion-modulated backscattered signal at each carrier frequency is calculated as $|S_r(f)|^2$ where $S_r(f) = \text{FFT}\{s_r(t)\}$ and the differential backscattered power from the motion-modulated chipless tag is obtained as

$$P_{bs\,d}(f_0) = \int_{-\infty}^{-\epsilon} |S_r(f)|^2\, df \; + \int_{+\epsilon}^{+\infty} |S_r(f)|^2\, df \tag{18}$$

for $f_0 = f_0^i$, $i = 1, 2, ..., N$ where $[-\epsilon, \epsilon]$ is the zero-excluding integration bandwidth like what is defined in (15). Finally, based on the differential backscattered power given in (18), the measured differential RCS at each carrier frequency f_0 is expressed as

$$\sigma_d(f_0) = \frac{(4\pi)^3 d^4\, P_{bs\,d}(f_0)}{\lambda^2 G_r G_t P_t} \tag{19}$$

for $f_0 = f_0^i$, $i = 1, 2, ..., N$ where G_t and G_r are respectively the gain of the TX and RX antennas.

Assuming the FFT calculation time negligible compared to the sweep time $t_{sw}^{(TS)}$ and the data transfer time $t_{tr}^{(TS)}$, the identification time $t_{ID}^{(TS)}$ required to complete the classical reading process based on VNA measurement in CW-TS mode can be calculated by

$$t_{ID}^{(TS)} = N \times [t_{sw}^{(TS)} + t_{tr}^{(TS)}] = N \times [(m \times t_{spm}) + t_{tr}^{(TS)}] \tag{20}$$

where $t_{spm} \propto 1/bw_{IF}$ and $t_{tr}^{(TS)} \propto m$. Thus, the three important parameters that define the identification time in motion-modulated chipless RFID based on the classical reading approach are respectively the number of requested frequency points N (which depends on the coding bandwidth BW of the chipless tag), the required time sweep $t_{sw}^{(TS)}$ that should lasts for several periods of motion, and the IF bandwidth set on the VNA (bw_{IF}) which should be determined respect to the motion period T_h. However, the most important result from (20) is that the identification time is linearly proportional to N which means, the greater the coding bandwidth, the longer is the identification time. For example, to identify a hand gesture-modulated chipless tag with a motion period of $T_h = 0.5$ sec over a coding bandwidth of $BW = 1$ GHz at $N = 100$ frequency points, supposing the sweep time of $t_{sw}^{(TS)} = 5 \times T_h = 2.5$ sec and transfer time $t_{tr}^{(TS)}$ of several 10 ms, the required identification time calculated using (20) is more than 250 seconds which is not at all feasible for a real RFID application. Accordingly, the very long identification time (about a few minutes), especially for slow motions with relatively large periods (more than a few 100 ms), is the main drawback of the classical reading approach (which is realized here based on VNA measurements in CW-TS mode) for motion-modulated chipless RFID. However, in contrast to the reader bench used in [17], [21], [23]–[26], [29] based on the synchronized signal generator-spectrum analyzer setup, the built-in coherent frequency sweep acquisition capability of a VNA can be effectively utilized to propose a novel reading method for motion-modulated chipless RFID in which the identification time can be significantly reduced for slow motion cases like hand gestures. This novel approach is discussed in the next section.

D. Frequency-Sweep Frozen-Time Approach Based on VNA

The novel proposed reading process for motion-modulated chipless RFID based on the Frequency-Sweep Frozen-Time (FS-FT) approach is realized using a VNA in FS mode and it is illustrated in Fig. 6 (c). The basic idea in this approach is to use the fast frequency sweep functionality of a VNA to acquire the motion-modulated backscattered signal during very short time slots compared to the motion period ($t_{sw}^{(FS)} << T_h$) such that the data associated with a large number of frequency points is acquired by a sequence of frequency sweeps. In this way, the acquisition in successive fast frequency sweeps can be used to reconstruct the motion-modulated signal samples during time for all the frequency points while the total identification time is significantly reduced. As it is shown in Fig. 6 (c), the VNA in FS mode sends N frequency points f_0^i, $i = 1, 2, ..., N$ at Port 1 during each frequency sweep [shown as $R1(f)$ with red impulses in Fig. 6 (c)] and acquires $[S_{21}]$ in Port 2 at the

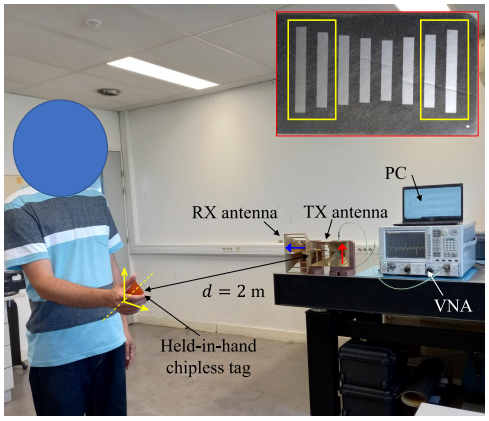

Fig. 7. Measurement setup in a real closed environment for hand gesture-modulated chipless RFID. The fabricated prototype of the chipless tag with $w_s = 30$ mm, $l_s = 50$ mm, $h_d = 18$ μm, $w = 2.5$ mm, $l_1 = 24$ mm, $l_2 = 22$ mm, $l_3 = 20$ mm, and $l_4 = 18$ mm is shown in the inset.

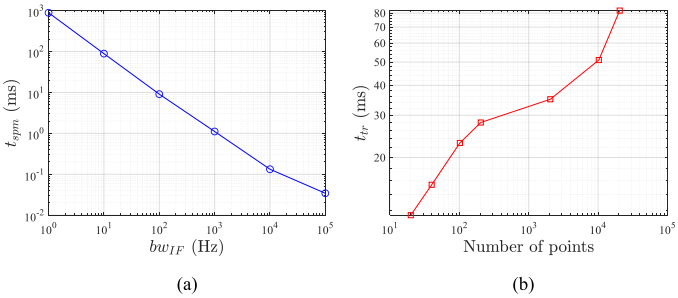

Fig. 8. Measured timing parameters of Keysight PNA N5222A. (a) Single point measurement time as a function of IF bandwidth. (b) Data transfer time from the VNA to the PC as a function of number of transferred data points.

corresponding N frequency points [shown as $S_{21}(f)$ with blue color in Fig. 6 (c)] during the sweep time of $t_{sw}^{(\mathrm{FS})}$. In contrast to the classical reading approach, as it is shown by yellow color on the motion trajectory in Fig. 6 (c), the sweep time $t_{sw}^{(\mathrm{FS})}$ is much smaller than the period of movement ($t_{sw}^{(\mathrm{FS})} << T_h$). This is why the proposed approach is called "Frequency-Swept Frozen-Time" referring that the frequency sweep acquisition is done while the moving chipless tag can be assumed frozen in time during $t_{sw}^{(\mathrm{FS})}$. To capture the motion-modulated signal for several periods of motion, the frequency sweep (with N frequency points) is done successively for m times to obtain m samples of the backscattered signal during motion for all frequency points. Indeed, compared to the classical approach where for N frequency points the CW-TS acquisition is done sequentially to obtain m signal samples in time, the FS-FT approach is arranged in a revers manner where to obtain m signal samples in time, the frequency sweep acquisition is done sequentially for m times with N frequency points in the sweep. However, after each frequency sweep, the data acquired for N frequency points should be transferred to the PC during $t_{tr}^{(\mathrm{FS})}$ as it is shown by black color on the motion trajectory in Fig. 6 (c). Accordingly, the equivalent sampling rate in FS-FT approach is $SR^{(\mathrm{FS})} = 1/[t_{sw}^{(\mathrm{FS})} + t_{tr}^{(\mathrm{FS})}]$ which should respect the Nyquist–Shannon sampling criterion based on the period of motion T_h. Note that the sweep time is $t_{sw}^{(\mathrm{FS})} = N \times t_{spm}$ where $t_{spm} \propto 1/bw_{IF}$ and the transfer time $t_{tr}^{(\mathrm{FS})} \propto N$. Therefor, the number of frequency sweep points N and the bw_{IF} should be chosen such that the equivalent sampling time of $t_{sw}^{(\mathrm{FS})} + t_{tr}^{(\mathrm{FS})}$ is much smaller than the period of motion T_h. After that the successive frequency sweep acquisitions is done for m times, the samples of the motion-modulated received signal $s_r(t)$ at each frequency points ($f_0 = f_0^i$, $i = 1, 2, ..., N$) are reconstructed based on the in-column arrangement of the acquired samples as it shown by shaded green bars and green paths in Fig. 6 (c). Accordingly, the complex received motion-modulated signal $s_r(t)$ in FS-TS approach at each frequency point can be obtained as

$$s_r(t_q)\Big|_{@\, f_0^i} = \sqrt{P_t}\, S_{21}(f_0^i)\Big|_{@t_q} \qquad (21)$$

for $q = 1, 2, ..., m$ and $i = 1, 2, ..., N$ where $t_q = (q-1)\,[t_{sw}^{(\mathrm{FS})} + t_{tr}^{(\mathrm{FS})}]$. Similar to the classical approach, by applying FFT to the obtained $s_r(t)$ at each frequency points, the PSD of the motion-modulated signal $|S_r(f)|^2$ is calculated and based on that, the measured differential RCS of the motion-modulated chipless tag at each frequency point is reached using (18) and (19).

Worth mentioning that, the main difference between the classical and the FS-FT approaches is that, in classical approach the differential RCS of the tag at each frequency point can be calculated immediately after the time sweep acquisition, whereas for FS-FT approach the differential RCS of the tag cannot be calculated for any frequency point until the end of m times frequency sweep acquisition. In addition, in the classical approach the sampling rate is just a function of bw_{IF} which can be controlled arbitrarily, while the sampling rate in FS-FT approach is a function of both bw_{IF} and the transfer time ($SR^{(\mathrm{FS})} = 1/[(N \times t_{spm}) + t_{tr}^{(\mathrm{FS})}]$). According to the usual transfer times of a few 10 ms, it is concluded that the sampling rate in FS-FT approach is mostly limited by the transfer time (and not by the bw_{IF}) and it cannot go beyond several 10 Hz. Thus, the FS-FT approach can be successfully applied for motion-modulated chipless RFID based on slow motions with a period greater than one-tenth of a second (equivalently with motion frequencies of less than 10 Hz). This fact should not count as a limitation for the FS-FT approach while most of the common natural movements in real life (like human body motions and objects carried by conveyor belts) produce modulation frequencies of less than several Hz.

The most important advantage of the FS-FT approach compared to the classical approach is addressed in terms of identification time. Similarly by neglecting the FFT calculation time, the total identification time of a motion-modulated chipless tag based on the FS-FT approach can be expressed as

$$t_{ID}^{(\mathrm{FS})} = m \times [t_{sw}^{(\mathrm{FS})} + t_{tr}^{(\mathrm{FS})}] = m \times [(N \times t_{spm}) + t_{tr}^{(\mathrm{FS})}] \qquad (22)$$

which is the required time to successively do the frequency sweep acquisition of N points (covering the coding bandwidth BW of the tag) for m times to capture all the data points needed to measure the differential RCS of the tag. For the same example with $T_h = 0.5$ sec, $BW = 1$ GHz, and $N = 100$, both the frequency sweep time $t_{sw}^{(\mathrm{FS})}$ and the transfer time $t_{tr}^{(\mathrm{FS})}$

can be around a few 10 ms (let's say 50 ms in summation), with $m = 100$, the data associated with ten periods of motion is captured while the achieved total identification time can be only $t_{ID}^{(FS)} = 5$ seconds. This is a great reduction compared to $t_{ID}^{(TS)} = 250$ seconds of identification time based on the classical approach. Indeed, equation (22) explicitly demonstrates that, in the FS-TS approach, the total identification time (m times of frequency sweep) should be around several periods of motion whereas in the classical approach, the time sweep at each frequency point (which is done N times) should last for several periods of motion. Accordingly, the FS-FT reading approach using VNA measurements proposes an effective solution to realize a fully practical motion-modulated chipless RFID system based on natural slow motions like hand gestures. It should be mentioned that, although the FS-FT approach is demonstrated here using VNA, it can be generally implemented based on a dedicated reader design (e.g. the data transfer time can be removed in an optimized design) while even much better performances can be achieved in terms of identification time.

IV. Results and Discussion

A. Measurement in Real Environment

The measurement setup for motion-modulated chipless RFID based on hand gesture in a real closed environment is illustrated in Fig. 7 where the Port 1 and Port 2 of the VNA (Keysight PNA Network Analyzer N5222A) is respectively connected to the TX and RX antennas (A.H. Systems SAS-571) and the $[S_{21}]$ parameter is measured. The TX and RX antennas are configured in cross-polarization and closely positioned to realize the mono-static scattering measurement. A prototype of the designed chipless tag has been fabricated on the ROGERS RT/duroid 5880 substrate with $\epsilon_r = 2.2$, $\tan\delta = 0.0004$, and $h_s = 0.508$ mm using normal PCB technology with 8 grounded-dipole REPs as it is shown in the inset of Fig. 7. The whole coding bandwidth of the fabricated chipless tag is $[3 : 6]$ GHz. The first four resonances of the chipless tag are considered in this measurement which are associated with the grounded-dipoles marked by the yellow boxes in Fig. 7 that occupy the acquisition bandwidth of $BW = [4.2 : 5.2]$ GHz. The geometrical characteristics of the four grounded-dipole REPs and the fabricated chipless tag are indicated in the caption of Fig. 7. A human subject holds the chipless tag in his hand with depolarizing configuration and performs the three gestures (Gesture 1, Gesture 2, and Gesture 3) in accord with the described trajectories presented in Fig. 1 at the distance d from the antennas. The period of all hand gestures is tried to be around $T_h = 0.8$ sec and the gesture characteristics are also tried to be compatible with the typical values indicated in Table II. The output power of the VNA is P_t and the VNA is controlled by a PC (DELL Latitude 7490 Core i7). The PC defines the parameters of the CW-TS and FS mode respectively in classical approach and FS-FT approach and also measures the sweep t_{sw} and transfer t_{tr} time at each step using timing functions of MATLAB. Fig. 8 presents the measured timing properties of Keysight PNA N5222A where Fig. 8 (a) shows the single point measurement time t_{spm} as a function of IF bandwidth bw_{IF} and Fig. 8 (b) shows the transfer time t_{tr} as a function of number of points (in CW-TS or FS mode) at $bw_{IF} = 1$ kHz. It should be mentioned that, although the maximum available IF bandwidth in N5222A is 15 MHz, to have enough SNR in reception, the data shown in Fig. 8 (a) is limited for bw_{IF} up to 100 kHz. In addition, the transfer time t_{tr} is almost independent of IF bandwidth and consequently, it has been measured in a typical $bw_{IF} = 1$ kHz using SCPI over TCP/IP protocol. As it was described in Section III and it is observed respectively in Fig. 8 (a) and (b), t_{spm} is inversely proportional to bw_{IF} and t_{tr} is directly proportional to the number of transferred data points.

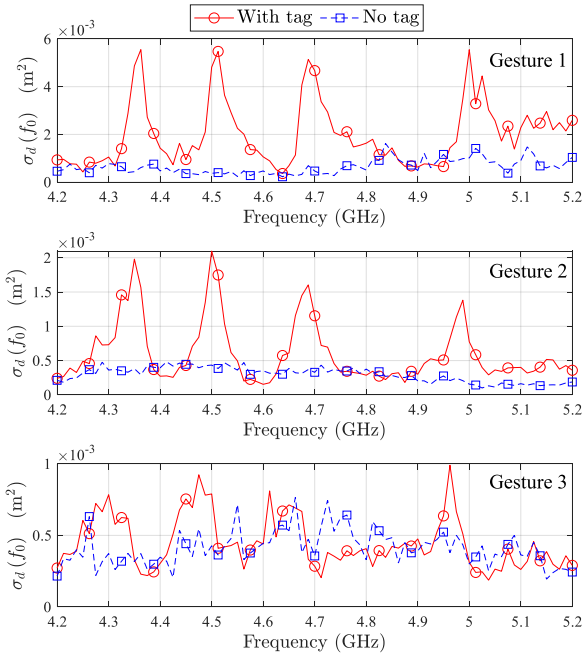

Fig. 9. Measured differential RCS of the hand gesture-modulated chipless tag in the three gestures.

TABLE III
VNA Measurement Parameters

	Classical approach	FS-FT approach
BW	1 GHz	1 GHz
N	81	81
m	3000	50
bw_{IF}	1 kHz	1 kHz
t_{sw}	$t_{sw}^{(TS)} = 2.8$ s	$t_{sw}^{(FS)} = 74$ ms
t_{tr}	$t_{tr}^{(TS)} = 54$ ms	$t_{tr}^{(FS)} = 31$ ms
t_{ID}	$t_{ID}^{(TS)} = 230$ s	$t_{ID}^{(FS)} = 5.7$ s

B. Identification Performance

The differential RCS of the hand gesture-modulated chipless tag is measured over $BW = [4.2 : 5.2]$ GHz using the described VNA measurement setup for the three gestures based on both the classical and FS-FT reading approaches. The measurement parameters for both approaches are indicated in Table III while the respective timing parameters have been measured by the PC. As the most important result, the achieved identification time based on FS-FT approach

($t_{ID}^{(FS)} = 5.7$ sec) is reduced by a factor of 40 compared to what is reached using classical reading approach ($t_{ID}^{(TS)} = 230$ sec). This is a great advancement in terms of identification time for slow motion-modulated chipless RFID which is realized here using hand gestures. Worth mentioning that, all the measured timing parameters for both approaches are in accord with the data given in Fig. 8 and the measured identification times $t_{ID}^{(TS)}$ and $t_{ID}^{(FS)}$ are respectively in agreement with what can be predicted using (20) and (22).

For $P_t = 10$ dBm and $d = 1$ m, the measured differential RCS of the hand gesture-modulated chipless tag has been obtained using (19) and (21) based on FS-FT approach for the three gestures which are shown in Fig. 9 as a function of carrier frequency. The measurement has been done in each gesture for two cases: 1) when the human subject holds the chipless tag in hand and performs the gestures (called as "With tag" in Fig. 9) and 2) when the human subject performs the gestures without holding the tag in hand (called as "No tag" in Fig. 9). According to the results shown in Fig. 9, the first four resonance of the hand gesture-modulated chipless tag can be perfectly identified in all three gestures based on the measured differential RCS which verifies the identification capability. Obviously, due to the depolarizing configuration of the hand gesture-modulated chipless tag, the cross-polarized differential RCS of the tag is significantly higher than that of the hand itself which enhance the detection robustness. In addition, the respective order of the measured differential RCS for the three gestures is in accord with what was predicted by the model and indicated in Table II in terms of MIME. In fact, since the MIME of Gesture 3 is quite lower than that of Gesture 1 and Gesture 2, the identification performance is a little bit degraded in Gesture 3 as shown in Fig. 9.

C. Hand Gesture Recognition

The gesture recognition capability based on motion-modulated chipless RFID is experimentally verified with the results shown Fig. 10. The IQ components of the motion-modulated received signal at the first resonance frequency of the chipless tag $f_0 = 4.35$ GHz is captured during 2.5 sec for each gesture at the distance of $d = 2$ m with $P_t = 10$ dBm, and the corresponding IQ diagrams are shown in Fig. 10 for each hand gesture during one period of motion ($T_h \approx 0.8$ sec). Note that, the IQ data shown in Fig. 10 are obtained based on FS-FT approach with the measurement parameters indicated in Table III which yields a sampling rate of $SR^{(FS)} = 1/[74\text{ ms} + 31\text{ ms}] = 9.5$ S/s. However, to show the measured IQ diagrams more precisely in Fig. 10, the captured samples are interpolated with a factor of 4 to have more data points of the IQ components. Similar to Fig. 4, on the selected period of gestures in Fig. 10, the start and end points are respectively marked with triangle and square marker in both the IQ variation plot and the IQ path diagram. The measured IQ trajectories shown in Fig. 10 for each gesture is in agreement with what has been obtained using model that have been shown in Fig. 4. Moreover, clearly different deterministic IQ trajectories associated with each hand gesture (respectively circular, linearly double round-trip, and semi-linearly single round-trip for Gesture 1, Gesture 2, and Gesture 3), proves the hand gesture recognition using the motion-modulated chipless RFID. Note that, the repetitive profile of the IQ components in the time domain representation (left side figures in Fig. 10) associated with the period of each gesture verifies the repeatability of the gesture recognition process using held-in-hand chipless tags.

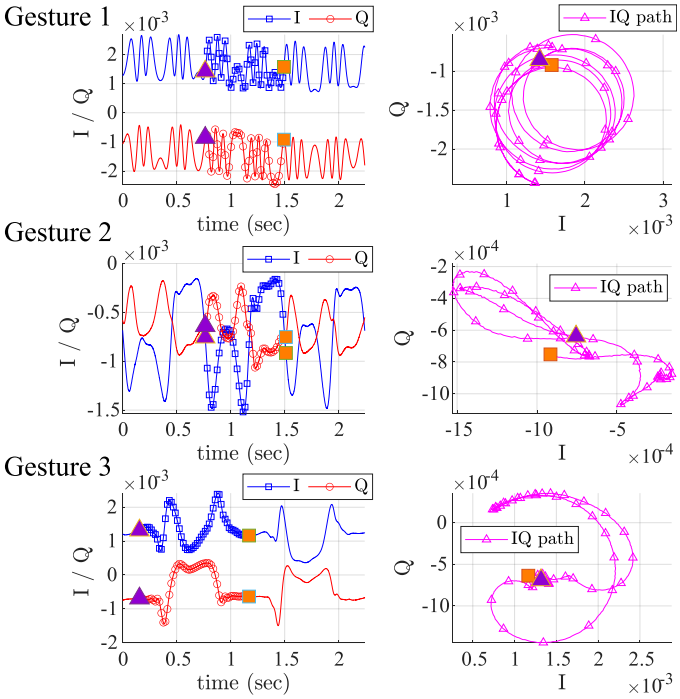

Fig. 10. Measured IQ components of the motion-modulated backscattered signal with corresponding IQ trajectories in the three gestures which can be applied for gesture recognition.

D. Maximum Achievable Read Range

Assuming that the hand itself has no cross-polarized backscattering component, the maximum reading distance of the hand gesture-modulated chipless tag can be easily predicted using radar equation as

$$d_{max} \leq \sqrt[4]{\frac{P_t G_t G_r \lambda^2 \sigma_d(f_0)}{(4\pi)^3 P_{r\,min}}} \tag{23}$$

where $P_{r\,min}$ is the IQ transceiver sensitivity and $\sigma_d(f_0)$ is the measured differential RCS shown in Fig. 9. For example, for Gesture 1 the differential RCS of the moving chipless tag at the resonance frequencies is about $\sigma_d \approx 6\times10^{-3}$ m^2 which yields the maximum read range of $d_{max} = 11.5$ m for $P_t = 10$ dBm and $P_{r\,min} = -95$ dBm. However, in a real situation, the cross-polarized backscattering component of the hand itself is not negligible which directly affects the maximum achievable read range. To demonstrate this fact, the PSD of the received signal $|S_r(f)|^2$ in Gesture 1 at the first resonance frequency of the tag $f_0 = 4.35$ GHz is measured using FS-FT approach (with the measurement parameters indicated in Table III, $P_t = 10$ dBm, $bw_{IF} = 1$ kHz, and at $d = 1$ m) in three cases as shown in Fig. 11 (a). The three cases are respectively "With

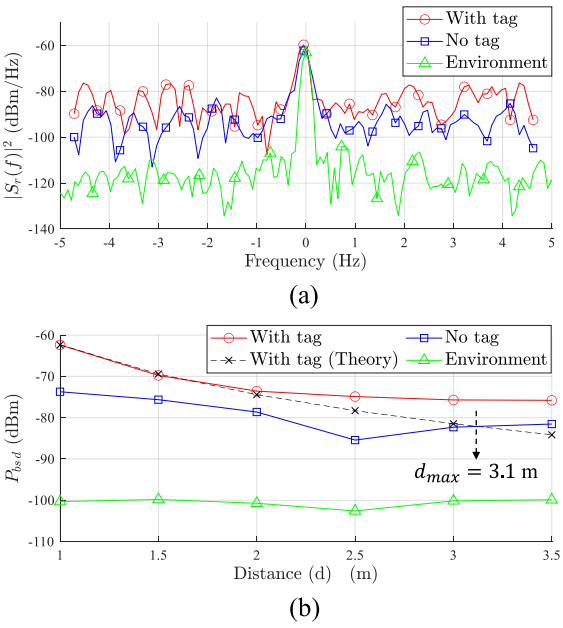

Fig. 11. (a) The measured PSD of the motion-modulated backscattered field in Gesture 1 at the first resonance frequency of the tag for two cases where the tag is held by hand and there is no tag in hand. (b) Measured differential backscattered power in Gesture 1 at the first resonance frequency as a function of distance.

tag", "No tag", and "Environment" where the two former are those already defined in the previous part and the latter is associated with the backscattering from environment when the human subject and his hand do not move at all. As it can be observed in Fig. 11 (a), although the level of the PSD in "With tag" case is higher than "No tag" case, the cross-polarized differential backscattered power from the hand itself is not negligible at all, which means at larger distances this undesired modulated power can limit the detection range of the chipless tag. This fact is illustrated by the results shown in Fig. 11 (b) where the differential backscatter power $P_{bs\,d}$ associated with the three cases is measured as a function of distance using (18). While $P_{bs\,d}$ of the stationary "Environment" is much lower than that of "With tag" case, $P_{bs\,d}$ of "No tag" case (generated by the hand itself in Gesture 1) is getting close to that of "With tag" at larger distances which limits the detection range. Accordingly, to predict the maximum achievable read range in Gesture 1, $P_{bs\,d}$ of "With tag" case is also theoretically calculated based on the radar equation shown as "With tag (Theory)" case in Fig. 11 (b). The point where $P_{bs\,d}$ of "With tag (Theory)" case intersects with that of "No tag" case determines the maximum achievable reading distance of $d_{max} = 3.1$ m for Gesture 1. Using the same procedure, the maximum achievable read range of the other gestures can be also predicted.

Finally, Fig. 12 presents the measured differential RCS of the hand gesture-modulated chipless tag in the three gestures at their maximum achievable read range which are respectively $d = 3$ m, $d = 2$ m , and $d = 1.5$ m for Gesture 1, Gesture 2, and Gesture 3 with $P_t = 10$ dBm. The four resonances of the chipless tag are successfully identified in the three gestures while they are shown by red arrows in Fig. 12.

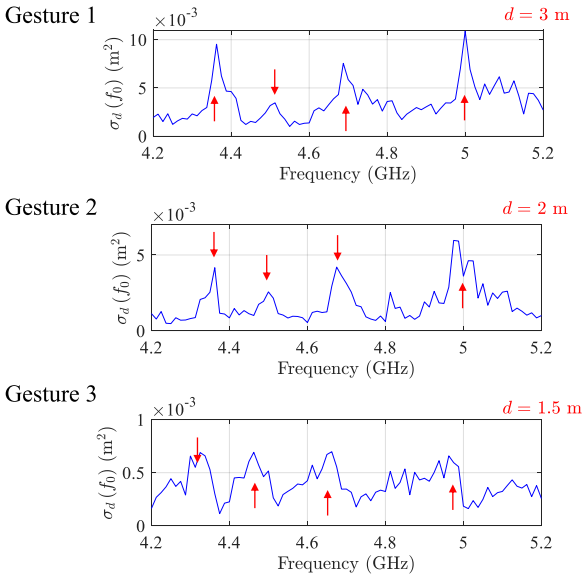

Fig. 12. Measured differential RCS of the hand gesture-modulated chipless tag in the three gestures where the chipless tag is identified at the corresponding maximum achieved read range.

V. Conclusion

The real-time identification of slow motion-modulated chipless tags based on hand gestures has been realized using the FS-FT reading approach. The FS-FT reading process has been demonstrated to reduce the identification time with a factor of 40 compared to the classical reading approach. The hand gesture-modulated chipless RFID based on three hand gestures have been analytically modeled while different kinds of motion-induced modulation (micro-Doppler, polarization, and directional amplitude modulation) were considered in each gesture. The identification capability based on the differential RCS has been verified by experiments in a real environment for all the gestures with an identification time of about 6 seconds. The hand gesture recognition capability has been addressed based on the obtained deterministic IQ signatures in each gesture and the concept has been verified by measurement for three different hand gestures at 2 m range. Finally, the maximum achievable read range for hand gesture-modulated chipless tags has been discussed while the tag has been identified at 3 m distance with the most efficient gesture.

Acknowledgment

This work was supported by the European Research Council (ERC) through the European Union's Horizon 2020 Research and Innovation Program (ScattererID) under Grant N° 772539.

References

[1] S. Preradovic and N. C. Karmakar, "Chipless RFID: Bar code of the future," *IEEE Microwave Magazine*, vol. 11, no. 7, pp. 87–97, 2010.
[2] R. Rezaiesarlak and M. Manteghi, *Chipless RFID*. Springer, 2016.
[3] O. Rance, E. Perret, R. Siragusa, and P. Lemaitre-Auger, *RCS synthesis for chipless RFID: theory and design*. Elsevier, 2017.
[4] L. Q. H. Nguyen and E. Perret, "Life cycle assessment of UHF and chipless RFID," in *2023 IEEE 13th International Conference on RFID Technology and Applications (RFID-TA), Aveiro, Portugal*. IEEE, 2023.

[5] S. Preradovic, I. Balbin, N. C. Karmakar, and G. F. Swiegers, "Multiresonator-based chipless RFID system for low-cost item tracking," *IEEE Trans. Microw. Theory*, vol. 57, no. 5, pp. 1411–1419, 2009.

[6] F. Costa, S. Genovesi, and A. Monorchio, "A chipless RFID based on multiresonant high-impedance surfaces," *IEEE Trans. Microw. Theory Tech.*, vol. 61, no. 1, pp. 146–153, 2013.

[7] A. Vena, E. Perret, and S. Tedjini, "Chipless RFID tag using hybrid coding technique," *IEEE Trans. Microw. Theory Tech.*, vol. 59, no. 12, pp. 3356–3364, 2011.

[8] L. Wang, T. Liu, J. Sidén, and G. Wang, "Design of chipless RFID tag by using miniaturized open-loop resonators," *IEEE Trans. Antennas Propag.*, vol. 66, no. 2, pp. 618–626, 2018.

[9] X. Wang, Y. Tao, J. Sidén, and G. Wang, "Design of high-data-density chipless RFID tag embedded in QR code," *IEEE Trans. Antennas Propag.*, vol. 70, no. 3, pp. 2189–2198, 2021.

[10] R. Rezaiesarlak and M. Manteghi, "Short-time matrix pencil method for chipless RFID detection applications," *IEEE Trans. Antennas Propag.*, vol. 61, no. 5, pp. 2801–2806, 2013.

[11] F. Costa, M. Borgese, A. Gentile, L. Buoncristiani, S. Genovesi, F. A. Dicandia, D. Bianchi, A. Monorchio, and G. Manara, "Robust reading approach for moving chipless RFID tags by using ISAR processing," *IEEE Trans. Microw. Theory Tech.*, vol. 66, no. 5, pp. 2442–2451, 2017.

[12] A. Ramos, E. Perret, O. Rance, S. Tedjini, A. Lázaro, and D. Girbau, "Temporal separation detection for chipless depolarizing frequency-coded RFID," *IEEE Trans. Microw. Theory Tech.*, vol. 64, no. 7, pp. 2326–2337, 2016.

[13] S. Jeong, J. Hester, R. Bahr, and M. M. Tentzeris, "A machine learning approach-based chipless RFID system for robust detection in real-world implementations," in *2021 IEEE MTT-S International Microwave Symposium (IMS)*. IEEE, 2021, pp. 661–664.

[14] N. Barbot, O. Rance, and E. Perret, "Classical RFID versus chipless RFID read range: Is linearity a friend or a foe?" *IEEE Trans. Microw. Theory Tech.*, vol. 69, no. 9, pp. 4199–4208, 2021.

[15] H. Stockman, "Communication by means of reflected power," *Proceedings of the IRE*, vol. 36, no. 10, pp. 1196–1204, 1948.

[16] P. Nikitin, "Leon Theremin (Lev Termen)," *IEEE Antennas and Propagation Magazine*, vol. 54, no. 5, pp. 252–257, 2012.

[17] A. Azarfar, N. Barbot, and E. Perret, "Motion-modulated chipless RFID," *IEEE Journal of Microwaves*, vol. 3, no. 1, pp. 256–267, 2022.

[18] M. S. Reynolds, "A 500 C° tolerant ultra-high temperature 2.4 GHz 32 bit chipless RFID tag with a mechanical BPSK modulator," in *2017 IEEE International Conference on RFID (RFID)*. IEEE, 2017, pp. 144–148.

[19] V. C. Chen, F. Li, S.-S. Ho, and H. Wechsler, "Micro-Doppler effect in radar: phenomenon, model, and simulation study," *IEEE Trans. Aerosp. Electron.*, vol. 42, no. 1, pp. 2–21, 2006.

[20] A. Lazaro, M. Lazaro, R. Villarino, and P. De Paco, "New radar micro-Doppler tag for road safety based on the signature of rotating backscatters," *IEEE Sensors J.*, vol. 21, no. 6, pp. 8604–8612, Mar. 2021.

[21] A. Azarfar, N. Barbot, and E. Perret, "Chipless RFID based on micro-Doppler effect," *IEEE Trans. Microw. Theory*, vol. 70, no. 1, pp. 766–778, 2021.

[22] N. Barbot and E. Perret, "Linear time-variant chipless RFID sensor," *IEEE Journal of Radio Frequency Identification*, vol. 6, pp. 104–111, 2021.

[23] A. Azarfar, N. Barbot, and E. Perret, "Directional amplitude backscatter modulation with suppressed Doppler based on rotating resonant loop," *Scientific Reports*, vol. 12, no. 1, p. 22032, 2022.

[24] ——, "Vibration sensing using Doppler-modulated chipless RFID tags," in *2022 IEEE/MTT-S International Microwave Symposium-IMS 2022*. IEEE, 2022, pp. 129–132.

[25] ——, "Long-range chipless RFID for objects in translation using Doppler-modulated depolarizing tags," in *2023 IEEE/MTT-S International Microwave Symposium-IMS 2023*. IEEE, 2023, pp. 1073–1076.

[26] ——, "Respiration monitoring using Doppler-modulated depolarizing chipless tags," in *2022 IEEE 12th International Conference on RFID Technology and Applications (RFID-TA)*. IEEE, 2022, pp. 149–152.

[27] P. Nikitin, K. Rao, and R. Martinez, "Differential RCS of RFID tag," *Electron. Lett.*, vol. 43, pp. 431 – 432, 02 2007.

[28] N. Barbot, O. Rance, and E. Perret, "Differential RCS of modulated tag," *IEEE Trans. Antennas Propag.*, vol. 2, no. 9, pp. 10–15, 2021.

[29] A. Azarfar, N. Barbot, and E. Perret, "Time-efficient reading process for motion-modulated chipless RFID," in *2023 IEEE 13th International Conference on RFID Technology and Applications (RFID-TA)*, 2023, pp. 53–56.

[30] S. Hemour and N. Barbot, "Backscattering modulation 101: VNA measurements," in *2023 IEEE 13th International Conference on RFID Technology and Applications (RFID-TA)*. IEEE, 2023, pp. 169–172.

[31] J. Lien, N. Gillian, M. E. Karagozler, P. Amihood, C. Schwesig, E. Olson, H. Raja, and I. Poupyrev, "Soli: Ubiquitous gesture sensing with millimeter wave radar," *ACM Transactions on Graphics (TOG)*, vol. 35, no. 4, pp. 1–19, 2016.

[32] T. Fan, C. Ma, Z. Gu, Q. Lv, J. Chen, D. Ye, J. Huangfu, Y. Sun, C. Li, and L. Ran, "Wireless hand gesture recognition based on continuous-wave Doppler radar sensors," *IEEE Trans. Microw. Theory*, vol. 64, no. 11, pp. 4012–4020, 2016.

[33] G. Li, R. Zhang, M. Ritchie, and H. Griffiths, "Sparsity-driven micro-Doppler feature extraction for dynamic hand gesture recognition," *IEEE Trans. Aerosp. Electron.*, vol. 54, no. 2, pp. 655–665, 2017.

[34] T. Sakamoto, X. Gao, E. Yavari, A. Rahman, O. Boric-Lubecke, and V. M. Lubecke, "Hand gesture recognition using a radar echo I–Q plot and a convolutional neural network," *IEEE sensors letters*, vol. 2, no. 3, pp. 1–4, 2018.

[35] M. G. Amin, Z. Zeng, and T. Shan, "Hand gesture recognition based on radar micro-Doppler signature envelopes," in *2019 IEEE radar conference (radarconf)*. IEEE, 2019, pp. 1–6.

[36] S. Franceschini, M. Ambrosanio, S. Vitale, F. Baselice, A. Gifuni, G. Grassini, and V. Pascazio, "Hand gesture recognition via radar sensors and convolutional neural networks," in *2020 IEEE Radar Conference (RadarConf20)*. IEEE, 2020, pp. 1–5.

[37] Y. Zhang, S. Dong, C. Zhu, M. Balle, B. Zhang, and L. Ran, "Hand gesture recognition for smart devices by classifying deterministic Doppler signals," *IEEE Trans. Microw. Theory*, vol. 69, no. 1, pp. 365–377, 2020.

[38] N. Barbot and E. Perret, "Gesture recognition with the chipless RIFD technology," in *2017 XXXIInd General Assembly and Scientific Symposium of the International Union of Radio Science (URSI GASS)*. IEEE, 2017, pp. 1–3.

[39] L. Shahid, H. Shahid, M. A. Riaz, S. I. Naqvi, M. S. Khan, Y. Amin, J. Loo *et al.*, "Chipless RFID tag for touch event sensing and localization," *IEEE Access*, vol. 8, pp. 502–513, 2019.

[40] R. Unnikrishnan, O. Rance, N. Barbot, and E. Perret, "Chipless RFID label with identification and touch-sensing capabilities," *Sensors*, vol. 21, no. 14, p. 4862, 2021.

[41] Z. Ali, N. Barbot, and E. Perret, "Gesture recognition using chipless RFID tag held in hand," in *2022 IEEE/MTT-S International Microwave Symposium - IMS 2022*, 2022, pp. 40–43.

[42] A. Azarfar, N. Barbot, and E. Perret, "Hand motion-modulated chipless RFID for gesture recognition," in *2024 IEEE/MTT-S International Microwave Symposium-IMS 2024*, 2024.

[43] A. Vena, E. Perret, and S. Tedjini, *Chipless RFID based on RF encoding particle: realization, coding and reading system*. Elsevier, 2016.

[44] A. Vena, E. Perret, and S. Tedjni, "A depolarizing chipless RFID tag for robust detection and its FCC compliant UWB reading system," *IEEE Trans. Microw. Theory*, vol. 61, no. 8, pp. 2982–2994, 2013.

Ashkan Azarfar (Member, IEEE) received the B.Sc. from the Iran University of Science and Technology, Tehran, Iran in 2014, and the M.Sc. from the University of Tehran, Tehran, Iran in 2017, both in electrical engineering. He received his Ph.D. degree from the University of Grenoble Alpes, Grenoble INP, France, in 2023. His thesis focused on the motion-modulated chipless RFID approach for long-range applications. He is currently a post-doctoral researcher at Grenoble INP, LCIS laboratory in Valence, France.

His current research is focused on signal processing methods in backscattering analysis for identification and sensing using chipless RFID tags.

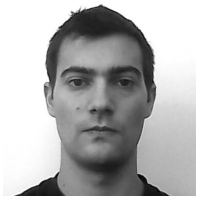

Nicolas Barbot (Member, IEEE) received the M.Sc. and Ph.D. degrees from the University de Limoges, France, in 2010 and 2013 respectively. His Ph.D. work in Xlim Laboratory, Limoges, France was focused on error-correcting codes for the optical wireless channel. He also realized a post-doctoral work in joint source-channel decoding at L2S Laboratory, in Gif-sur-Yvette, France. Since September 2014, he has been an Assistant Professor at the Université Grenoble Alpes - Grenoble Institute of Technology, in Valence, France. His scientific background at LCIS Laboratory, Valence, France covers wireless communications systems based on backscattering principle which include classical RFID and chipless RFID.

His research interests include transponders which can not be described by linear time-invariant systems. This gathers harmonic transponders which are based on the use of a non-linear component (Schottky diode) or linear time-variant transponders which are based on the modification of their response in the time domain. He also places special interests on antenna design and instrumentation based on these phenomenons.

Etienne Perret (Senior Member, IEEE) received the Eng. Dipl. degree in electrical engineering from the Ecole Nationale Supérieure d'Electronique, d'Electrotechnique, d'Informatique, d'Hydraulique, et des Télécommunications, Toulouse, France, 2002, and the M.Sc. and Ph.D. degrees in electrical engineering from the Toulouse Institute of Technology, Toulouse, in 2002 and 2005, respectively. From 2005 to 2006, he held a post-doctoral position with the Institute of Fundamental Electronics, Orsay, France. He was appointed Associate Professor in 2006 and Full Professor in 2022 of electrical engineering at Univ. Grenoble Alpes, Grenoble INP, France, where he heads the ORSYS Research Group (20 researchers) from 2015 to 2022. From 2014 to 2019, he has been a Junior Member with the Institut Universitaire de France, Paris, France, an institution that distinguishes professors for their research excellence, as evidenced by their international recognition. From 2015 to 2020, he has been an appointed Member of the French National Council of Universities. He has authored or co-authored more than 200 technical conferences, letters and journal papers, and books and book chapters. He holds several patents. His works have generated more than 4200 citations. His current research interests include wireless communication systems based on the principle of backscatter modulation or backscattering of EM waves especially in the field of RFID and chipless RFID for identification and sensors. His research interests also include electromagnetic modeling of passive devices for millimeter and submillimeter-wave applications, and advanced computer-aided design techniques based on the development of an automated codesign synthesis computational approach. Dr. Perret has been a Technical Program Committee member of the IEEE International Conference on RFID, the IEEE RFID TA; and currently he is a member of the IMS Technical Paper Review Committee. He was a recipient of several awards like the MIT Technology Review's French Innovator's under 35 in 2013, the French Innovative Techniques for the Environment Award in 2013, the SEE/IEEE Leon Brillouin Award for his outstanding achievement in the identification of an object in an unknown environment using a chipless label or tag in 2016, the IEEE MTT-S 2019 Outstanding Young Engineer Award, the Prix Espoir IMT – Académie des sciences in 2020 and the Grand Prix de l'Electronique Général Ferrié in 2021. He was a Keynote Speaker and the Chairperson of several international symposiums. Etienne Perret was awarded an ERC Consolidator Grant in 2017 for his project ScattererID.